Bull. Mater. Sci., Vol. 39, No. 3, June 2016, pp. 729–735. © Indian Academy of Sciences.
DOI 10.1007/s12034-016-1199-6

Effects of calcium impurity on phase relationship, ionic conductivity and microstructure of Na^+-β/β″-alumina solid electrolyte

SUNG-TAE LEE, DAE-HAN LEE, SANG-MIN LEE, SANG-SOO HAN, SANG-HYUNG LEE and SUNG-KI LIM*

Department of Materials Chemistry and Engineering, Konkuk University, 120 Neungdong-ro, Gwangjin-gu, Seoul 143-701, South Korea

MS received 28 May 2015; accepted 28 December 2015

Abstract. **Ca-doped Na^+-β/β″-alumina was synthesized using a solid-state reaction. The changes in the properties of Na^+-β/β″-alumina resulting from the presence of Ca impurity were studied. Ca (0–5 wt%) was added to the respective samples, which were then sintered. The specimens were characterized using X-ray diffraction, scanning electron microscopy, densimetry and impedance analysis. In the sintered specimens, the β″-alumina phase fraction decreased as Ca content increased, whereas the relative sintered density increased. The surface morphology of Ca-doped Na^+-β/β″-alumina specimens showed a Ca-rich layer, which was the main cause of increase in the specific resistance.**

Keywords. **Na^+-β/β″-alumina; solid electrolyte; calcium impurity; specific resistance.**

1. Introduction

Since its development in the 1980s, the Na/S battery has been one of the most promising candidates for energy storage applications. The Na/S battery functions based on the electrochemical reaction between sodium and sulphur to form sodium polysulphide, and exhibits high power and energy density, temperature stability; furthermore, it is inexpensive, because of its abundant lowcost raw materials and is suitable for high-volume mass production. The battery is composed of a sodium anode, a sulphur cathode, and Na^+-β/β″-alumina as both the electrolyte and separator [1,2]. Na^+-β/β″-alumina ceramics come from two parent phases designated as β-alumina and β″-alumina, which have resistivities of 30 and 5 Ω·cm, respectively, at 350°C. The β-alumina phase has the theoretical formula $Na_2O \cdot 11Al_2O_3$ or $NaAl_{11}O_{17}$ [3], and the β″-alumina phase has the formula $Na_2O \cdot 5Al_2O_3$, or $NaAl_5O_8$ [4]. According to the Na_2O–Al_2O_3 phase diagram proposed by Fally *et al* [5], the β and β″ phases coexist in the region corresponding to the formula $Na_2O \cdot nAl_2O_3$ ($5.33 \leq n \leq 8.5$). The crystalline structure of β″-alumina is rhombohedral with an R3m space group and lattice constants of $a = 5.614$ and $c = 33.85$ Å. Generally, the a-axis is similar to that of the β-alumina structure, but the c-axis is 1.5 times longer and the concentration of alkaline ions on the conduction plane is higher. Therefore, β″-alumina shows a much higher ionic conductivity [6,7].

Generally, Na^+-β/β″-alumina powder is synthesized through a conventional solid-state reaction and the precursors usually employed are sodium and lithium carbonate and aluminium oxides of the α- or γ-form [8,9]. Commercial aluminium oxides have many impurities, including Ca, Si, Zr and Fe. Ca and Si are well known as liquid-phase sintering promoters of α-alumina, but excessive Ca and Si form excess liquid phase, resulting in hindered contact between the particles and the formation of pores due to contraction of the generated gas during cooling, thereby hampering the sintering process [10,11]. Zr in Na^+-β/β″-alumina ceramics leads to an increase in mechanical strength and fracture toughness, but excess Zr causes a decrease in the ionic conductivity of Na^+-β/β″-alumina [12]. It was also found that low Fe doping increases the ionic conductivity of Na^+-β/β″-alumina [13]. Among these impurities, Ca is the most abundant. In recent years, numerous studies have focussed on understanding the effect of small amounts of Ca impurities on the sintering of ultra-pure α-alumina [14–16]. In addition, many research groups have reported on the influence of Ca impurities on the cycling behaviour of Na/S cells [17,18]. However, the effects of incorporating Ca as an impurity in Na^+-β/β″-alumina solid electrolytes during the powder synthesis step have not been well established. Thus, in this study, Ca-doped Na^+-β/β″-alumina specimens were fabricated and the changes in the properties of the Na^+-β/β″-alumina solid electrolyte resulting from the presence of Ca impurities were investigated.

2. Experimental

The Na^+-β/β″-alumina samples were synthesized through a conventional solid-state reaction. The molar ratio of $[Na_2O] : [Al_2O_3]$ was 1 : 5, and the MgO (stabilizer) content was fixed at 1.6 wt%. α-Al_2O_3 (99.99%, High Purity

*Author for correspondence (sklim@konkuk.ac.kr)

Chemicals, Japan), Na_2CO_3 (99+%, Sigma-Aldrich, USA) and $4MgCO_3 \cdot Mg(OH)_2 \cdot 5H_2O$ (99+%, Sigma-Aldrich, USA) were used as the starting materials for the Al_2O_3, Na_2O and MgO sources, respectively. To investigate the effects of Ca as an impurity in Na^+-β/β″-alumina, $CaCO_3$ was added during the Na^+-β/β″-alumina powder synthesis step, and

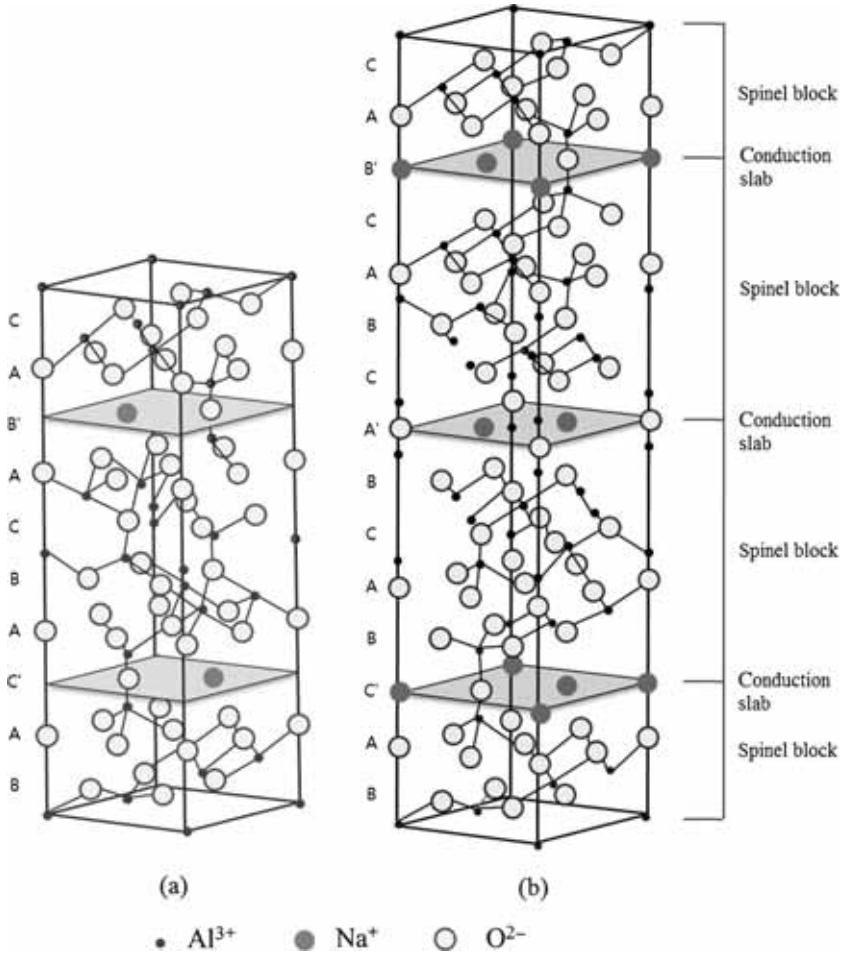

Figure 1. Perspective drawings of the idealized structures of (**a**) Na^+-β-alumina and (**b**) Na^+-β″-alumina [6,7].

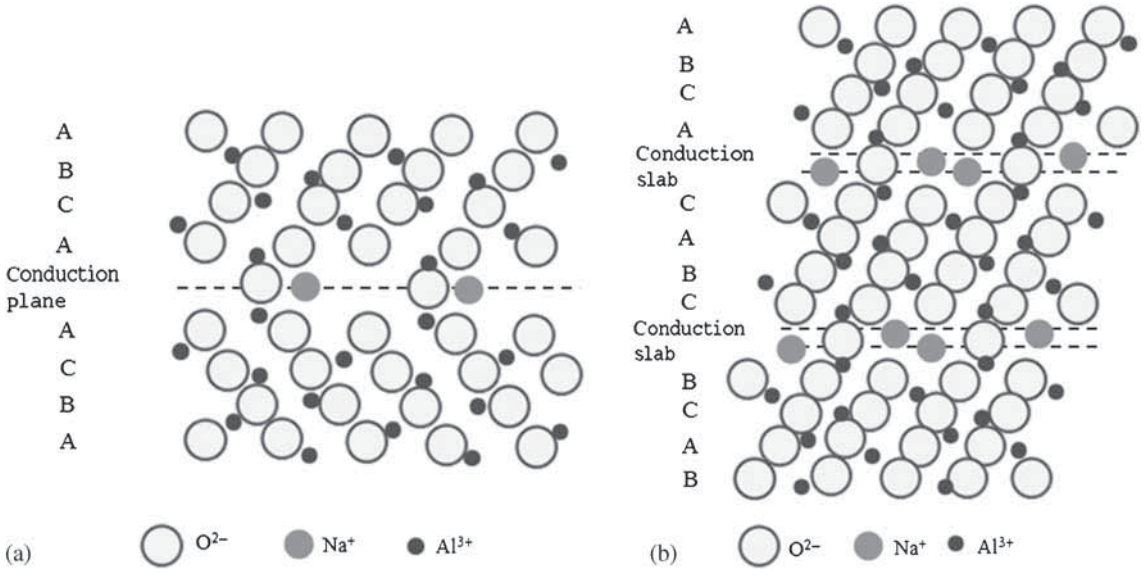

Figure 2. Stacking sequence upto the *c*-axis of (**a**) Na^+-β-alumina and (**b**) Na^+-β″-alumina [22].

the amount of Ca was varied from 0 to 5 wt%. α-Al_2O_3 was mixed with Na_2CO_3, $4MgCO_3 \cdot Mg(OH)_2 \cdot 5H_2O$ and $CaCO_3$ by ball-milling for 5 h using alumina balls ($\Phi = 5$ and 10 mm) and methanol as the liquid medium. Then, the mixture was dried at 90°C for 24 h, and the powders were calcined at 1200°C for 2 h. To prepare ultra-fine powders, the calcined powders were milled by attrition milling using zirconia balls ($\Phi = 1$ mm) with methanol as the medium. Each sample was prepared into tablet form via uniaxial pressing at 100 bar. To minimize Na_2O loss, the green samples were buried in MgO crucibles packed with the synthesized Na^+-β/β″-alumina and sintered at 1600°C for 30 min in an air atmosphere. After sintering, the microstructure of the powders was observed with a scanning electron microscope (Model JSM-6380, Japan), and the density was calculated via the Archimedes method (ASTM 373-88). The ionic conductivities of the sintered specimens were measured by blocking silver electrodes using an electrochemical complex impedance analyzer (Zahner, IM6), in the frequency range of 1 Hz to 3 MHz and temperature range of 25–350°C. The sodium conductivities were calculated using the equation

$$\sigma = \frac{L}{R_s \times A}, \tag{1}$$

where σ, L, R_s and A denote the ionic conductivity, specimen thickness, impedance of the specimen and electrode area, respectively.

The phase compositions of the calcined and sintered samples were measured with an X-ray diffractometer (D/max 2200, Rigaku, Japan). The relative amounts of the phases were determined by calculating the line intensities of the well-separated peaks of each phase using the following equations [19,20]:

$$\%\ \text{of}\ \alpha = \frac{f(\alpha)}{f(\alpha) + f(\beta) + f(\beta'')} \times 100, \tag{2}$$

$$\%\ \text{of}\ \beta = \frac{f(\beta)}{f(\alpha) + f(\beta) + f(\beta'')} \times 100, \tag{3}$$

$$\%\ \text{of}\ \beta'' = \frac{f(\beta'')}{f(\alpha) + f(\beta) + f(\beta'')} \times 100, \tag{4}$$

$$f(\alpha) = \frac{1}{2}\left\{ I_{\alpha(104)} \times \frac{10}{9} + I_{\alpha(113)} \right\}, \tag{5}$$

$$f(\beta) = \frac{1}{3}\left\{ I_{\beta(104)} \times \frac{10}{3} + I_{\beta(206)} \times \frac{10}{3.5} + I_{\beta(107)} \times \frac{10}{5.5} \right\}, \tag{6}$$

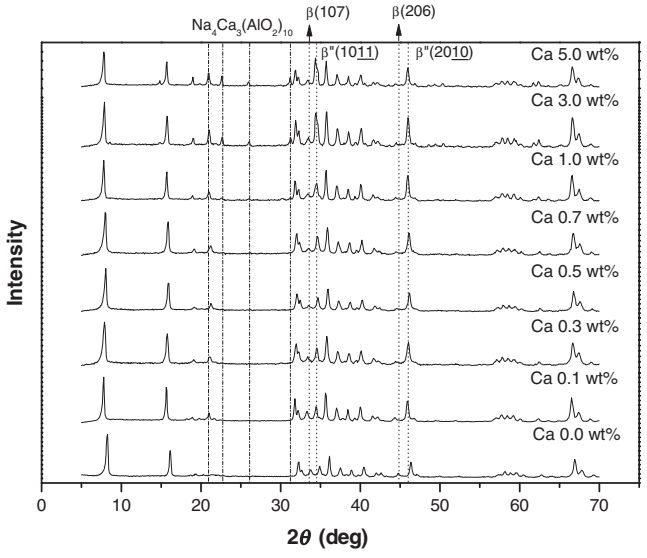

Figure 3. XRD patterns of the Na^+-β/β″-alumina powders calcined at 1200°C for 2 h with and without Ca.

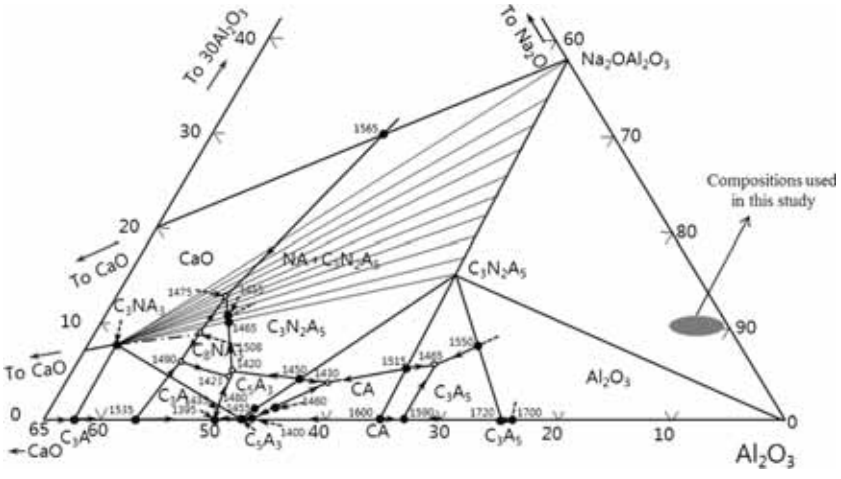

Figure 4. Na_2O–CaO–Al_2O_3 ternary phase diagram presented by Brownmiller and Bogue, C = CaO; A = Al_2O_3; N = Na_2O [23].

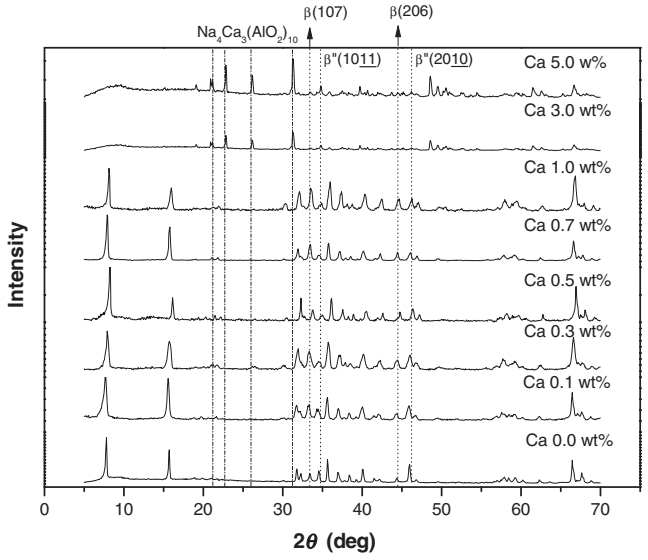

Figure 5. XRD patterns of the Na^+-β/β″-alumina specimens sintered at 1600°C for 30 min.

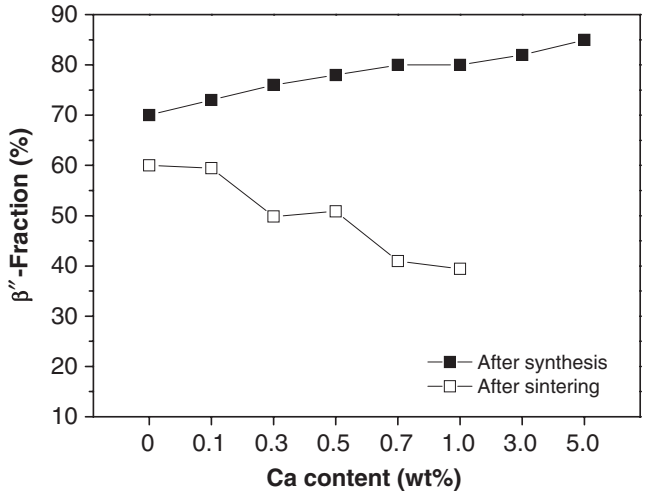

Figure 6. Phase fraction of the Na^+-β″-alumina of the synthesized powders and sintered specimens.

$$f(\beta'') = \frac{1}{2}\left\{ I_{\beta''(10\underline{1}1)} \times \frac{10}{4} + I_{\beta''(20\underline{1}0)} \times \frac{10}{8} \right\}, \qquad (7)$$

where $I_{\alpha(104),\ \alpha(113)}$ is X-ray intensities of the (104) and (113) planes of the α-alumina phase, $I_{\beta(102),\ \beta(206),\ \beta(107)}$ the X-ray intensities of the (102), (206) and (107) planes of the β-alumina phase and $I_{\beta''(111),\ \beta''(2010)}$ the X-ray intensities of the (10$\underline{1}$1) and (20$\underline{1}$0) planes of the β″-alumina phase.

3. Results and Discussion

Figure 1 shows schematic structures of β-alumina and β″-alumina, which contain a tightly packed spinel block and a loosely arranged conduction slab, where the sodium ions can conduct rapidly. Three spinel blocks are contained in each β″-alumina unit cell, while β-alumina has two spinel blocks

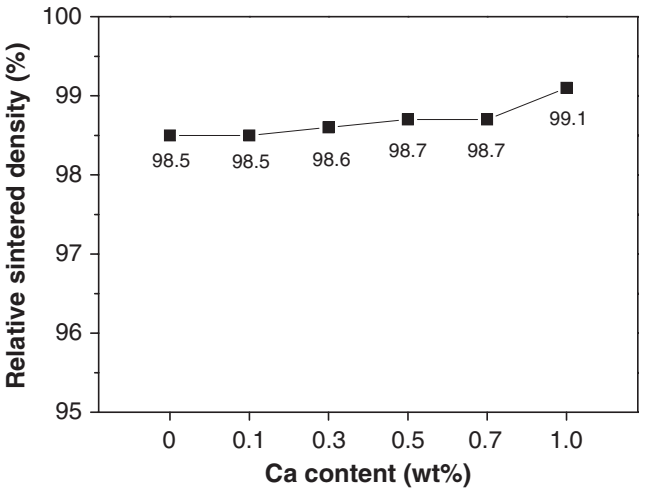

Figure 7. Relative sintered density of the sintered Na^+-β/β″-alumina specimens as a function of Ca content.

per unit cell. In the β-alumina structure, aluminium ions are in both the octahedral and tetrahedral sites. Generally, divalent cations (Ca^{2+}, Mg^{2+}, Co^{2+}, Mn^{2+}, Zn^{2+} and Fe^{2+}) strongly prefer a tetrahedral coordination environment in the β/β″-alumina structure [21]. Figure 2 shows the structure highlighting the stacking sequence of layers up to the *c*-axis of β-alumina and β″-alumina. The unit cell of β″-alumina is 50% larger than that of β-alumina by virtue of the difference in the stacking sequence. Adjacent close-packed oxide slabs are again held apart by Al–O–Al spacer units, but alternate sodium atom sites lie above and below the plane through the centre of the oxide spacer atoms, and the Na^+ ion diffusion path actually encompasses a finite volume (the conduction slab) rather than a plane as in the β-alumina structure. β″-alumina has a higher Na content in the conduction slab than β-alumina, and therefore is more conductive than β-alumina [22].

Figure 3 shows the XRD patterns of the synthesized Na^+-β/β″-alumina powders with and without Ca. All the XRD patterns of the synthesized powders appeared similar in shape with the growth of the (107), (206) planes and the (10$\underline{1}$1), (20$\underline{1}$0) planes corresponding to β- and β″-alumina, respectively. The β″-alumina peaks had higher intensities than the β-alumina peaks. The secondary phase of the Na_2O–Al_2O_3–CaO ternary system, the $Na_4Ca_3(AlO_2)_{10}$ phase appeared in all samples with the exception of the powder without Ca (Ca 0 wt%), and the $Na_4Ca_3(AlO_2)_{10}$ phase was clearly observed in the synthesized powders with 3 and 5 wt% Ca. The phase existing in the $Na_4Ca_3(AlO_2)_{10}$ composition was identified from the agreement of the diffraction pattern with that of JCPDS card No. 02-1003. The main diffraction lines of $Na_4Ca_3(AlO_2)_{10}$ at the d_{hkl} values of 4.19, 3.90, 3.40 and 2.83 Å corresponded to the d_{hkl} values in the present study.

Figure 4 shows the phase diagram for the ternary system Na_2O–CaO–Al_2O_3, produced by Brownmiller and Bogue [23]. The compositions used in this study are marked in figure 4; the $Na_4Ca_3(AlO_2)_{10}$ phase appeared according to

the phase diagram for the ternary Na_2O–CaO–Al_2O_3 system in these compositions. Figure 5 presents the XRD patterns of the sintered specimens. In the 0–1 wt% Ca-doped sintered specimens, no significant peaks corresponding to $Na_4Ca_3(AlO_2)_{10}$ were observed, which may be due to the volatilization of Na_2O, leading to the decomposition of $Na_4Ca_3(AlO_2)_{10}$, and the dissolution of Ca in the Na^+β/β″-alumina. $Na_4Ca_3(AlO_2)_{10}$ has an unstable phase and an intermediate phase between $CaO \cdot Al_2O_3$ and $Na_2O \cdot Al_2O_3$ [23]. In the case of the 3 and 5 wt% Ca-doped specimens, the β/β″-alumina phase was not maintained; it completely transformed to a $Na_4Ca_3(AlO_2)_{10}$ phase.

Figures 6 and 7 show the β″-alumina phase fraction analysis and the relative sintered density, respectively. Before sintering, the β″-alumina phase fraction increased as the Ca content increased, whereas after sintering, the β″-alumina fraction decreased as the Ca content increased. The dissolved Ca in the β/β″-alumina led to excessive volatilization of the Na_2O to adjust the charge balance of Na^+-β/β″-alumina. The relative sintered density increased slightly with the the addition of Ca. The increase in Ca content caused the formation of liquid phases during the sintering process [14], and this aided the densification of the Na^+-β/β″-alumina specimens.

Figure 8 shows the Nyquist plots of the 1 wt% Ca-doped sintered specimen and the specimen without Ca at 350°C. The measured resistance of the 1.0 wt% Ca-doped specimen was higher than that of the 0.0 wt% Ca-doped specimen. Further, the grain boundary contribution to the total electrolyte resistance was negligible above 250°C [22], and hence, the semicircle corresponding to the grain boundary was not observed at 350°C. The ionic conductivity of the specimens sintered at 1600°C for 30 min is shown in figure 9. In the case of the 3 and 5 wt% Ca-doped specimens, the β/β″-alumina phase was completely transformed to a $Na_4Ca_3(AlO_2)_{10}$ phase; hence, the ionic conductivity was not measured. Among the samples, the maximum ionic conductivity was measured for the specimen without Ca, i.e.,

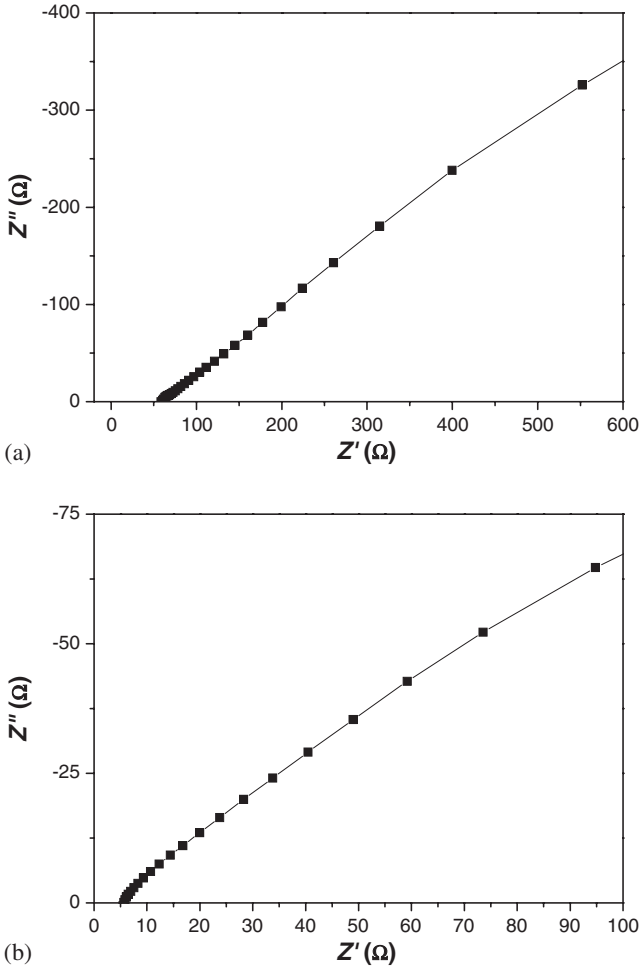

Figure 8. Nyquist plot of sintered Na^+-β/β″-alumina specimen: (**a**) with 1.0 wt% of Ca and (**b**) without Ca at 350°C.

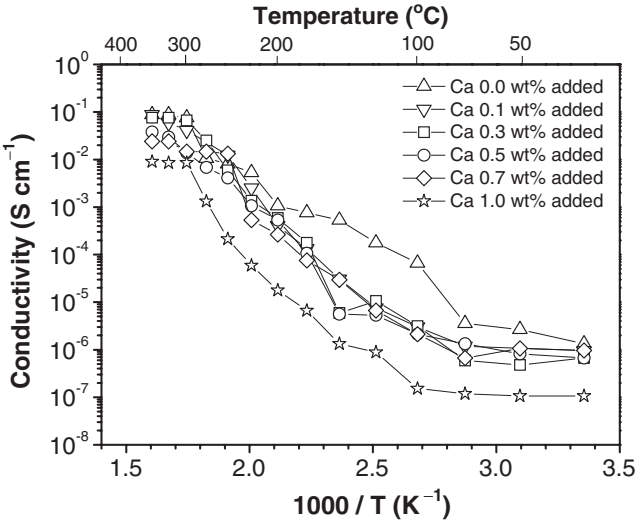

Figure 9. Ionic conductivity of sintered Na^+-β/β″-alumina specimens as a function of Ca content at 25–350°C.

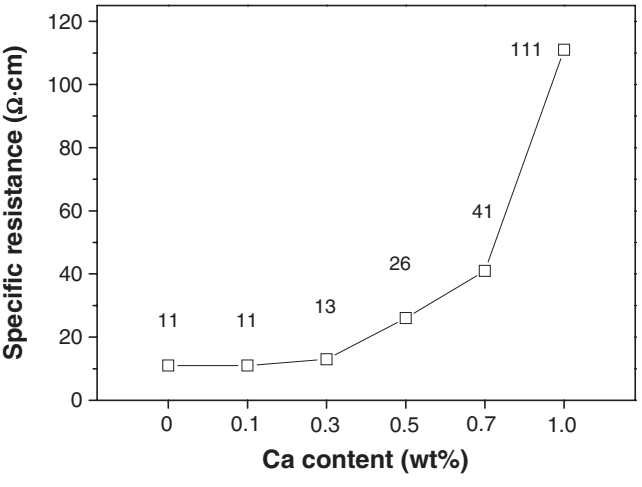

Figure 10. Specific resistance of sintered Na^+-β/β″-alumina specimens as a function of Ca content at 350°C.

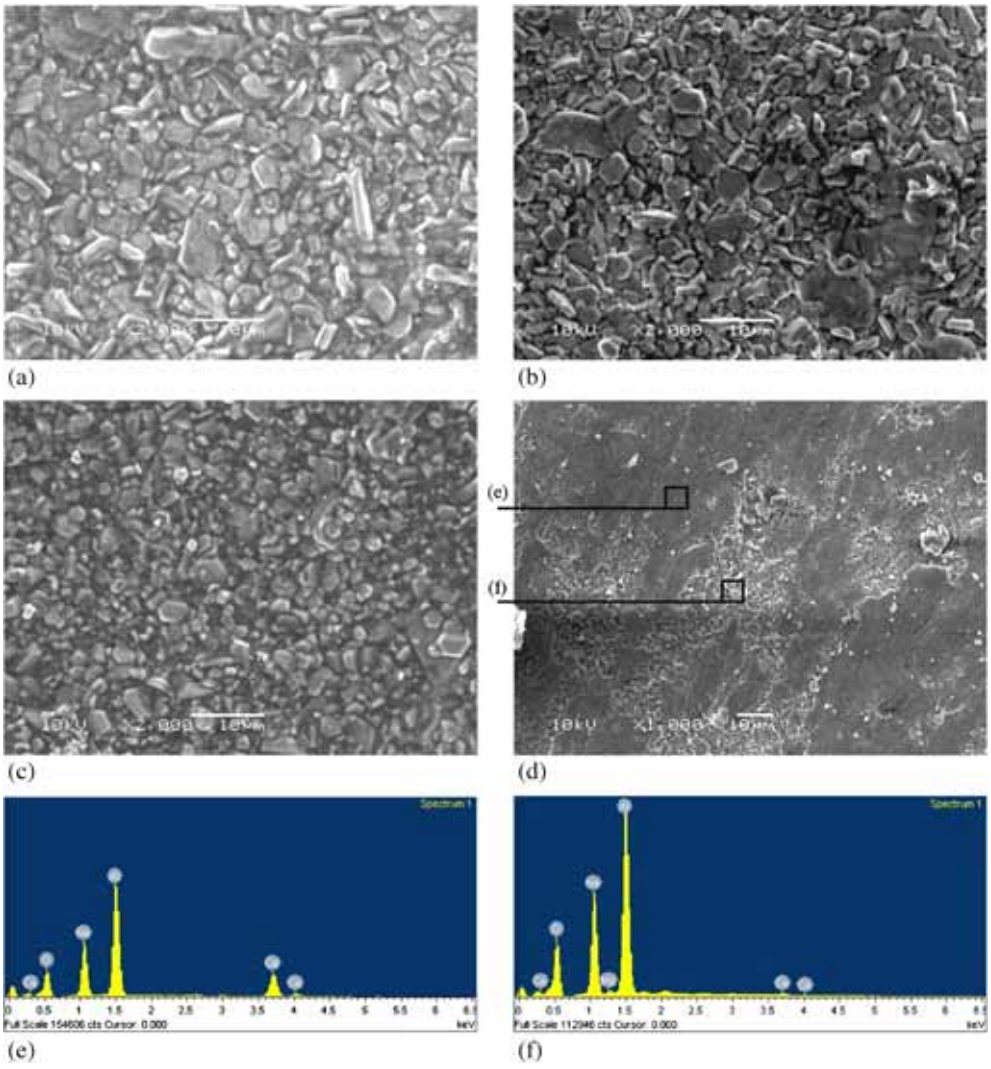

Figure 11. SEM images and EDX spectra of sintered Na^+-β/β″-alumina specimens: (**a**) 0.1 wt% Ca-doped specimen (×2000), (**b**) 0.5 wt% Ca-doped specimen (×2000), (**c**) 1.0 wt% Ca-doped specimen (×2000), (**d**) 1.0 wt% Ca-doped specimen (×1000), (**e**) EDX spectra of the covered and (**f**) uncovered layer regions.

8.8×10^{-2} S cm^{-1} at 350°C, and the minimum ionic conductivity was measured for the 1 wt% Ca-doped specimen, 9.0×10^{-3} S cm^{-1} at 350°C. The ionic conductivity decreased as the Ca content increased. Figure 10 shows the specific resistance of the sintered specimens. The specific resistance of the specimen without Ca was 11 Ω·cm at 350°C, and the value increased with increasing Ca content. In the case of the 1 wt% Ca-doped specimen, the specific resistance at 350°C, was 111 Ω·cm.

Figure 11 shows SEM images and EDX spectra of the sintered specimens. It can be clearly observed that the grain size tends to be smaller with increasing Ca content. It has been reported that Ca concentrates in the grain boundaries of β/β″-alumina [17], and it is considered to inhibit the growth of the grains. Figure 11c and d presents the surface morphologies of the 1 wt% Ca-doped Na^+-β/β″-alumina specimen. The morphology type in figure 11c was observed in most surface regions of the 1 wt% Ca-doped specimen, but the microstructures covering the layer in figure 11d were only partially observed. Therefore, the EDX spectra of the covered and non-covered layer regions in figure 11d are presented in figure 11e and f, respectively. The intensity of the Ca peak of the covered layer region is higher than that of the uncovered region, confirming that more Ca was distributed in the covered layer region. It has been reported that a Ca-rich layer is formed if Ca exists in β/β″-alumina, leading to an increase in Na^+-β/β″-alumina resistance [17,18].

4. Conclusions

In the present study, the properties of Ca-doped Na^+-β/β″-alumina were analysed. After calcination, a $Na_4Ca_3(AlO_2)_{10}$ phase was observed in all samples with the exception of

the powder without addition of Ca (0 wt% Ca). Because of the volatilization of Na_2O, the $Na_4Ca_3(AlO_2)_{10}$ phase was decomposed and Ca was dissolved in the Na^+-β/β″-alumina. In the sintered specimens, the β″-alumina phase fraction decreased with the addition of Ca. As Ca was added, a Ca-rich layer formed on the surface of the Na^+-β/β″-alumina specimen, mainly giving rise to an increase in specific resistance. The specific resistance of the specimen without Ca was 11 Ω·cm at 350°C, which indicated a tendency of the specific resistance to increase with increasing Ca content. In the case of the 1 wt% Ca-doped specimen, the specific resistance at 350°C was 111 Ω·cm. Conclusively, the properties of Na^+-β/β″-alumina were not affected by the addition of <0.1 wt% of Ca impurity.

Acknowledgements

This work was supported by the Energy Efficiency & Resources Core Technology Programme of the Korea Institute of Energy Technology Evaluation and Planning (KETEP) granted financial resources by the Ministry of Trade, Industry & Energy, Republic of Korea (No. 20142010102460).

References

[1] Ohsima T, Kajita M and Okuno A 2004 *Int. J. Appl. Ceram. Tec.* **1** 269

[2] Rydh C J and Sanden B A 2005 *Energy Convers. Manag.* **46** 1957

[3] Yao Y Y and Kummer J T 1967 *J. Inorg. Nucl. Chem.* **29** 2453

[4] Certo J, Furtado C S, Ferreira A J and Perdigao J M 1998 *Ionics* **4** 124

[5] Fally J, Lasne C, Lazennec Y, Le Cars Y and Margotin P 1973 *J. Electrochem. Soc.* **120** 1296

[6] Yamaguchi G and Suzuki K 1968 *Bull. Chem. Soc. Jpn.* **41** 93

[7] De Kroon A P, Schafer G W and Aldinger F 1995 *Chem. Mater.* **7** 878

[8] Schaefer G W, Van Zyl A and Weppner W 1990 *Solid State Ionics* **40–41** 154

[9] Kvachkov R, Yanakiev A, Poulieff C N, Balkanov J, Yankulov P D and Budevski E 1981 *J. Mater. Sci.* **16** 2710

[10] Svancarek P, Galusek D, Calvert C, Loughran F, Brown A, Brydson R and Riley F 2004 *J. Eur. Ceram. Soc.* **24** 3453

[11] Park S H, Park W J and Yoon H K 2008 *Trans. Korean Soc. Mech. Eng. A* **32** 1003

[12] Heavens S N 1988 *J. Mater. Sci.* **23** 3515

[13] Kennedy J H, Stuber S M and Parker S F 1983 *Solid State Ionics* **8** 323

[14] Brydson R, Twigg P C, Loughran F and Riley F L 2001 *J. Mater. Res.* **16** 652

[15] Tas A C 1998 *J. Am. Ceram. Soc.* **81** 2853

[16] Louet N, Epicier T and Fantozzi G 2006 *Key Eng. Mater.* **313–318** 1

[17] Yasui I and Doremus R H 1978 *J. Electrochem. Soc.* **125** 1007

[18] Breiter M W, Choudhury N S and Hall E L 1984 *Solid State Ionics* **14** 225

[19] Schimid C 1986 *J. Mater. Sci. Lett.* **5** 263

[20] Lee S T, Kim S G, Jang M H, Hwang S H, Haw J R and Lim S K 2010 *J. Ceram. Proc. Res.* **11** 86

[21] Xie L and Cormack A N 1990 *Mater. Lett.* **9** 474

[22] Sudworth J L and Tilley A R 1985 The sodium sulfur battery (London: Champman and Hall Ltd) Chap 2, p 21

[23] Brownmiller L T and Bogue R H 1932 *Am. J. Sci.* **23** 501